Hindawi
Shock and Vibration
Volume 2023, Article ID 6643622, 13 pages
https://doi.org/10.1155/2023/6643622

Research Article

Experimental Study on Hydrodynamic Performance of the Integrated Floating Breakwater-Wind Turbine Device

Jianting Guo,[1] **Renhao Wu**,[2] **Xubing Gao**,[1] **and Yuxin Yang**[1]

[1]*School of Naval Architecture and Ocean Engineering, Jiangsu University of Science and Technology, Zhenjiang 212003, China*
[2]*Marine Design and Research Institute of China, Shanghai 200011, China*

Correspondence should be addressed to Jianting Guo; 201600000072@just.edu.cn

Received 17 July 2023; Revised 2 September 2023; Accepted 22 September 2023; Published 29 September 2023

Academic Editor: FuRen Ming

This study presents the design of an integrated floating breakwater-wind turbine device. The hydrodynamic performance was evaluated in a two-dimensional water tank under typical operating conditions to investigate its kinematic response and wave dissipation effect, while the original design was improved and optimized to enhance the overall performance of the integrated device. The improved integrated device had lower heave and sway motion amplitudes, better wave resistance, and better wave dissipation performance than the prototype. The improved integrated device can effectively reduce costs and optimize the allocation of resources by using a floating breakwater as a carrier for wind power generation and has broad application prospects.

1. Introduction

Renewable energy is becoming increasingly important as the world focuses on climate issues and continues to invest in reducing carbon emissions and is dependent on fossil fuels. Wind is a vital source of clean, renewable energy, which can help in protecting the environment. Owing to its low cost and low pollution, wind power has become one of the fastest-growing renewable energy sources worldwide, with significant growth over the past decade [1]. Wind power is primarily classified into onshore and offshore sources. However, in recent years, offshore wind power projects, particularly floating wind turbine projects (FOWTs), have become increasingly popular owing to the pursuit of land utilization rates and power generation scales. Floating wind turbines can operate at different water depths and seabed conditions and have good economic benefits and broad market prospects [2]. Compared to traditional stationary offshore wind turbines, floating wind turbines are less affected by water, easy to install and disassemble, and have become the first choice for offshore wind power development in various countries [3].

In recent years, various energy companies and countries have actively invested in the research of new floating wind turbine configurations, and a variety of floating wind turbine design schemes have been proposed and verified, such as France's "Floatgen" ring floating wind turbine [4], Spain's "DemoSATH" double hull floating wind turbine project [5], and Sweden's "Windsea" three-tower floating wind turbine [6]. When designing a new configuration for a floating wind turbine, it is necessary to study its kinematic response in wind and wave environments. Jonkman [7], for example, established an equation for motile control based on the potential flow, blade element momentum, and dynamics of a multibody system and conducted aerodynamic and hydrodynamic coupling numerical simulations in combination with numerical algorithms. This method has become one of the most widely used research techniques in related fields and has been used in many practical applications, such as NREL's FAST simulation program [8] and DNV-GL Bladed [9]. In addition, scholars have tried other methods. Zhou et al. [10] used CFD to simulate the coupled aero-hydromooring FOWT, and the results showed that an increase of the wave steepness will lead to the nonlinear load arising at FOWT structure natural frequencies. Tran and Kim [11] used computational fluid dynamics (CFD) and multibody dynamic analysis methods based on potential energy to analyze the dynamic response of floating wind

turbines. The results showed that the simulation results correlated well with the experimental data. Yang et al. [12] studied the motion and load response of FOWT based on the blade element momentum theory and the potential flow theory and examined the precision of a middle-fidelity simulation tool (OrcaFlex). Shen et al. [13] mentioned that as empirical models are often used in numerical calculations, numerical simulations require model tests for verification and correction, which reduces the uncertainty of numerical simulations under nonlinear working conditions. For the mooring system of FOWT, scholars also have corresponding research. Li et al. [14] discussed the influence of different mooring modes on the dynamic response of FOWT in medium water depth, and the results indicated that the configuration with 4 tension legs and 12 mooring cables with an inclination angle of 30° is the most structurally stable mooring system under extreme sea state. Presently, in model tests, it is mainly used to ensure that the solid model satisfies Froude's law of proportionality and to use steel chains or springs to simulate mooring cables to achieve equivalent recovery stiffness and damping. The hydrodynamic loads of the floating wind turbine base were simulated with relative accuracy using a wave generator in the simulated pool. Because the two theorems of similarity cannot be satisfied simultaneously, the simulation of aerodynamic loads mainly relies on various methods to perform equivalent simulations of aerodynamic thrust and neglects secondary loads, such as aerodynamic torque [15, 16].

Breakwaters have played an important role in the construction of ports worldwide as essential devices for protecting ports and resisting waves. Researchers have recently developed various breakwaters to meet the protection needs under different sea and coastal conditions. It includes all types of fixed breakwaters, such as the semicircular membrane breakwater invented by Li et al. [17] and perforated caisson breakwater proposed by Liu et al. [18]. Sun et al. [19] developed a kelp-box-type floating breakwater. Although the traditional fixed breakwater has good reflection ability, it also has the disadvantages of time-consuming installation and construction, which are not conducive to exchanging internal and external water bodies. Compared with fixed breakwaters, floating breakwaters have advantages such as low engineering costs, effective water pollution prevention, strong adaptability to the environment, and broad application prospects [20, 21].

In the study of floating breakwaters, the hydrodynamic characteristics and other physical properties were primarily based on numerical analyses and pool tests of the model. Ji et al. [22] used flume model tests and numerical models to study the hydrodynamic characteristics and wave dissipation performance of a cylindrical double-pontoon floating breakwater. Compared to a single-pontoon floating breakwater, the former exhibits better wave dissipation performance, especially for waves with extended periods and large wave heights. Christensen et al. [23] conducted flume model tests and used the boundary integral method (BIEM) to study the hydrodynamic characteristics and wave dissipation performance of three types of floating breakwaters: a single tank, a single tank with wing plates, and a single tank with both wing plates and porous media. The single-float tank with wing plates significantly reduced the motion response, whereas the single-float tank with both wing plates and porous media exhibited the best wave suppression performance. In recent years, computational fluid dynamics (CFD) has been increasingly favored by researchers as a commonly used method for simulating the interactions between waves and floating structures. With improved simulation accuracy and lower computational costs, computational fluid dynamics (CFD) has become crucial for numerical model analyses. Currently, the finite volume method (FVM), which is based on grid and smoothed particle hydrodynamics (SPHs) methods, is primarily used in hydrodynamic research on floating breakwaters. Islam et al. [24] analyzed the wave radiation caused by the movement of a floating box-type breakwater using the finite volume method with the Open-FOAM open-source toolkit. Cui et al. [25] developed a floating breakwater with an open moon pond structure and studied its hydrodynamic characteristics using SPH. Compared with a single bucket-type floating breakwater, the new design configuration exhibits excellent wave dissipation performance.

In summary, domestic and foreign scholars have done a lot of research on floating offshore wind turbine and floating breakwater. The floating breakwater has been verified in wave elimination performance, and the FOWT has been increasingly maturing in power generation and stability. However, the integrated device combining floating breakwater and floating wind turbine has not been studied yet. Combining these two characteristics is of practical significance for designing a floating breakwater and wind turbine integration device with dual functions of wave dissipation and wind power generation. Based on the respective characteristics of the floating wind turbine and floating breakwater, a concept integrating a floating wind turbine and floating breakwater is proposed, which is beneficial for reducing construction costs and improving their respective economic performances. This study proposes an improved design scheme for integrated floating breakwater and wind turbine systems based on the existing scheme. An integrated floating breakwater, wind turbine device, and improved scheme were tested under constant wind and regular wave conditions. The wave elimination effect, motion response, and mooring force of the two devices were measured, and the feasibility of the integrated device was verified, laying a foundation for future integrated device tests for loading multiwind turbines or high-power wind turbines.

2. The Design Scheme of the Floating Breakwater and Wind Turbine-Integrated Device

The integrated floating breakwater and wind turbine device uses a double-cylindrical floating breakwater as the base. A circular cross brace connects the middle of the two cylindrical structures, and the base of the wind turbine tower is located on the middle cross brace [21, 26]. The integrated device realizes wind power generation using the upper wind turbine, and simultaneously, the double-cylindrical floating breakwater in the lower part can interfere with the waves and play a role in wave prevention and elimination.

This study presents the design parameters of this type of integrated device, the overall configuration of which is shown in Figure 1. The specific parameters of the floating breakwater are listed in Table 1. The wind power generator set was selected from a 5WM wind turbine (NREL-5WM) researched by the National Institute of Renewable Energy. This type of wind turbine is widely used in wind turbine research and manufacturing [27]. The specific parameters used are listed in Table 2.

To improve the overall performance of the integrated device, the original design was improved and optimized, and wing plates were installed on both sides of the double cylinder of the floating breakwater. The length and width of the wing plate were 40 m and 3 m. The proposed device aims to weaken the motion amplitude of the floating breakwater, improve its wave-absorbing effect, and simultaneously provide a more stable power-generation platform for the floating wind turbine to enhance the practicability of the integrated device. The configuration diagram of the improved integrated device is shown in Figure 2.

3. Physical Model Test Design

3.1. Model Similarity Design and Test Conditions. This experiment was conducted at Jiangsu University of Science and Technology using a two-dimensional water tank. The wave basin is 40 m long, 0.8 m wide, and 1.4 m deep. Combined with the practical section scale and wave-making capacity of the flume and the main scale of the integrated device, this test used the model scaling ratio $\lambda = 60$, and the test water depth is 1 m. There is a gap between the model and the water tank, and according to a large number of relevant studies, the error caused by this gap is considered acceptable [28]. The main parameters of the double-cylinder floating breakwater after scaling are listed in Table 3 and those of the anchor chain in the test are listed in Table 4.

In the process of wind turbine similarity design, when considering the aerodynamic load in a wind turbine model, the test design scheme of the mainstream wind turbine should first ensure that the simulation of the axial thrust of the blade is accurate. It is mainly divided into two simulation schemes: one simulates the load by restoring the wind turbine blade rotation, and the other simulates the force of the wind turbine equivalent. Restoring blade rotation mainly involves the movement of the wind turbine blade itself, spiral torque, and tower tremor it causes, to make every effort to truly restore the working state of the actual wind turbine as much as possible [29]. The equivalent simulation scheme is mainly used to study the overall performance of floating wind turbines and to conduct test research conveniently and quickly. In this study, an equivalent design scheme for the wind turbine thrust was adopted. In the specific test design, the equivalent method of wind area was not adopted to double the equivalent of wind turbine thrust, such as the thrust disk scheme adopted by Wan et al. [30]. Instead, a scheme in which the motor thrust replaces the thrust received by the wind turbine was adopted for the test design [31]. In this study, it was ensured that the reaction force generated by the blade rotation driven by the motor on the integrated device was equal to the axial thrust of the blade; therefore, the simulation of the aerodynamic load met the test requirements. Figure 3 shows the thrust curves of three classic full-size floating wind turbines. An NREL wind turbine was selected as the integrated device. During the test, the thrust was calibrated by adjusting the wind turbine speed of the culvert. The simulated wind speed under these test conditions was 11 m/s. According to the similarity criterion, the thrust in the test is 3.16 N, and the culvert fan used to thrust simulation is 50 mm EDF; the fan for the test is shown in Figure 4(a). The wing plate installation details for the improved integrated device are shown in Figure 4(b), the diagram of the experimental model is shown in Figure 5, and the integrated device model is shown in Figure 6. The length of the wing plate model is 0.67 m and the width is 0.05 m.

In these tests, the wind speed was set to 11 m/s. To study the change rule of the motion response amplitude and wave elimination effect of the integrated device under different wave heights and period changes, tests were conducted in different periods under the conditions of regular wave heights of 3 m and 4.5 m. The specific working conditions are listed in Table 5.

3.2. Test and Measurement Scheme. The coordinate system used to measure the effects of wave suppression and the motion responses of the sway, roll, and heave of the integrated equipment are shown in Figure 7. The measurement of the wave-elimination effect is shown in Figure 8. Five wave gauges were arranged, among which No. 1 was arranged 8 m in front of the model, mainly for calibrating the incident waves. Wave gauges 2 and 4 were arranged 3 m from the front and rear of the model, and wave gauges 3 and 5 were 0.4 m away from No. 2 and No. 4, respectively. Wave gauges 2 and 3 used the Goda two-point method to separate the incident waves [32]. Wave gauges 4 and 5 used the two-point method to separate the transmitted waves.

A noncontact optical motion measuring system was used to measure sway, roll, and heave. To ensure that the light sensor was not affected by the light-reflecting spot on the water surface, the light sensor was arranged at a height of 1.2 m above the floating breakwater model and rigidly connected to the wind turbine tower barrel with light materials. The specific arrangement is shown in Figure 6.

4. Test Results and Analysis

4.1. Model Test Phenomena. Typical test photographs of the improved integrated device during the test process under test condition 14 are shown in Figure 9. By comparing the test results with the archetype, the response duration curves of the three-degrees-of-freedom motions of sway, heave, and roll under the same working conditions are shown in Figure 10. The comparison curves of the rear-wave durations under these working conditions are shown in Figure 11.

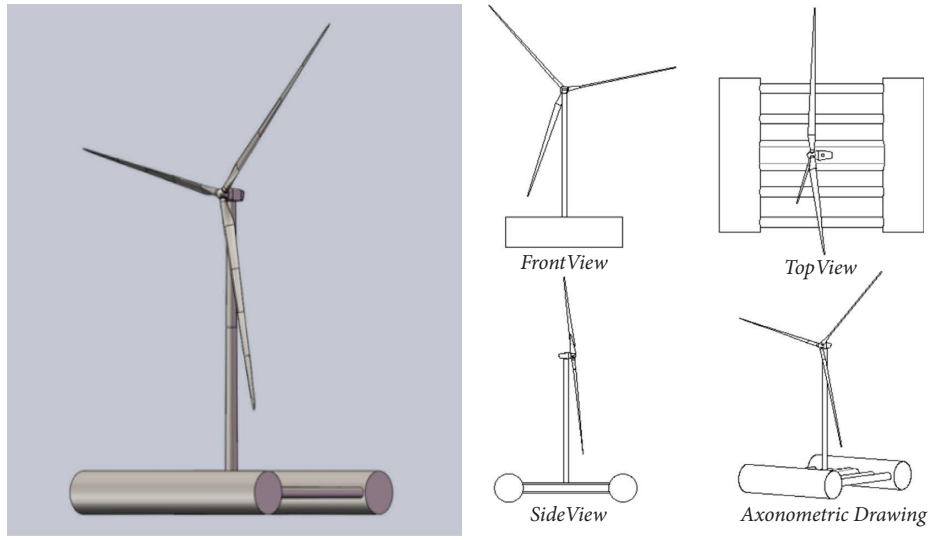

Figure 1: (a) Overall configuration of the integrated device; (b) projection of the original model in all directions.

Table 1: Main parameters of the archetype of the double-cylindrical floating breakwater.

Length (m)	L	45.6
Width (m)	B	60
Height (m)	D	12
Draft (m)	T	7
Diameter of pontoon (m)	D_1	12
Length of connector (m)	L_h	36
Diameter of connector (m)	D_h	3

Table 2: Parameters of NREL-5WM wind turbine.

Quantity of blades	3
Diameter of wind wheel	126 m
Rated wind speed	11.4 m/s
Working wind speed	(3–25) m/s
Height of tower	90 m

The comparison results in Figure 10 show that, under the interaction of wind and wave loads, the motion amplitude of the improved integrated device was smaller than that of the archetype in both the heave and sway directions. The sway and heave amplitudes decreased by 25.4% and 9.1%, respectively, and the roll amplitude was slightly larger than that of the archetype by 4.3%. The comparison results in Figure 11 show that the improved wave-attenuation effect was better than that of the original model, and the wave height behind the dike decreased by 22.3%. The improved reciprocating motion in the equilibrium position exhibited stable motion performance and a remarkable wave elimination effect. Compared with the archetype, the improved model exhibited better wave resistance in sway and heave, and the overall operation of the device was more stable.

4.2. Motion Response Analysis. To more intuitively show the influence of the heave motion response amplitude of the integrated device as the wave period changes and to study the effect of the improved device on reducing the heave amplitude, the variation in the heave amplitude with the period is shown in Figure 12.

According to the analysis in Figure 12, the heave amplitude of the improved device under the influence of the wave cycle was smaller than that of the archetype device under the same change and its amplitude decreased by 8% on average. Under a wave period $T < 1.4$ s, the heave amplitudes of both devices showed an upward trend, and the improved device showed a better antiheave and stability effect, which played a more critical role in maintaining the stable operation of the device itself. This was because the wing plate installed on the improved device produced additional mass and damping enhancement effects during movement, which effectively increased the restoring force of the device. When the wave period $T > 1.4$ s, the variation curves of both the heave amplitudes and period tended to be flat and consistent. This was because the heave motion of the device is intensified with an increase in the wave period. At this time, the continuously increasing buoyancy plays a leading role in the recovery force of the device itself, and the buoyancies of the two devices are equal, resulting in the extreme values of the sway amplitudes tending to be consistent.

To more intuitively show the influence of the oscillation motion response amplitude of the integrated device as the wave period changes and to study the effect of the improved device on reducing the sway amplitude, the variation in sway amplitude with the period is shown in Figure 13.

According to the analysis in Figure 13, it can be concluded that the modified and archetype devices have the same variation trend of the sway motion response amplitude under the influence of wave period changes. With an

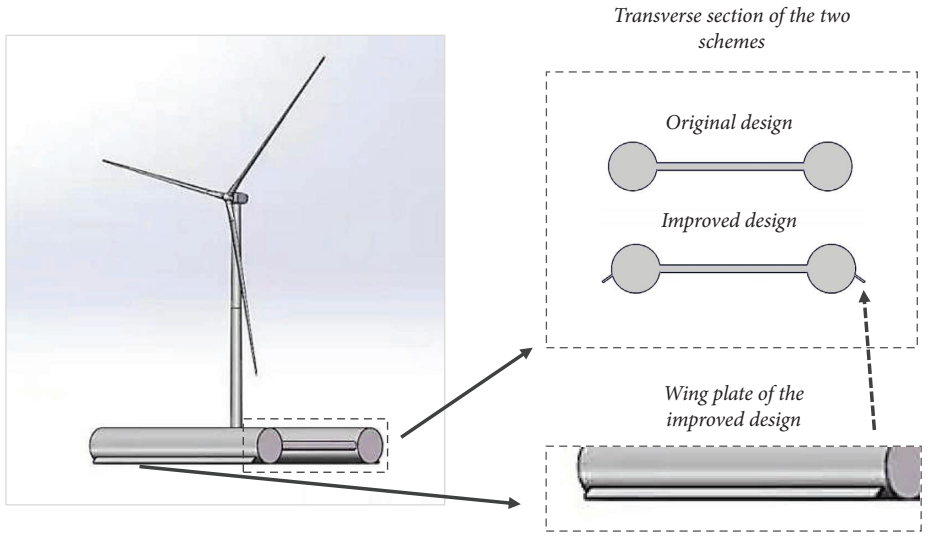

Figure 2: Configuration diagram of the improved integrated device.

Table 3: Main parameters of the floating breakwater model.

Length (m)	L	0.76
Width (m)	B	1
Height (m)	D	0.2
Draft (m)	T_1	0.115
Radius of mooring (m)	R	2.5
Diameter of pontoon (m)	D_1	0.2

Table 4: Mooring cable parameters in the test.

Name	Diameter (mm)	Length (m)	Axial rigidity (KN/m)	The submerged weight per unit length (g/m)
304 stainless steel chain	2.5	2.88	473.5	113

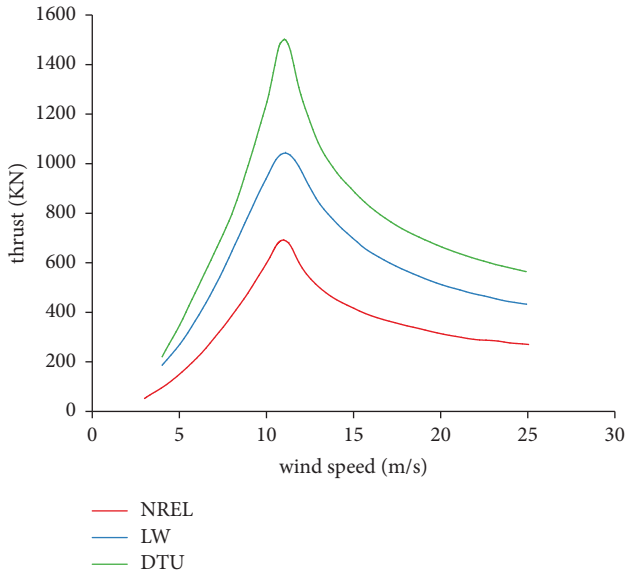

Figure 3: Thrust curves of three classic full-size floating wind turbines.

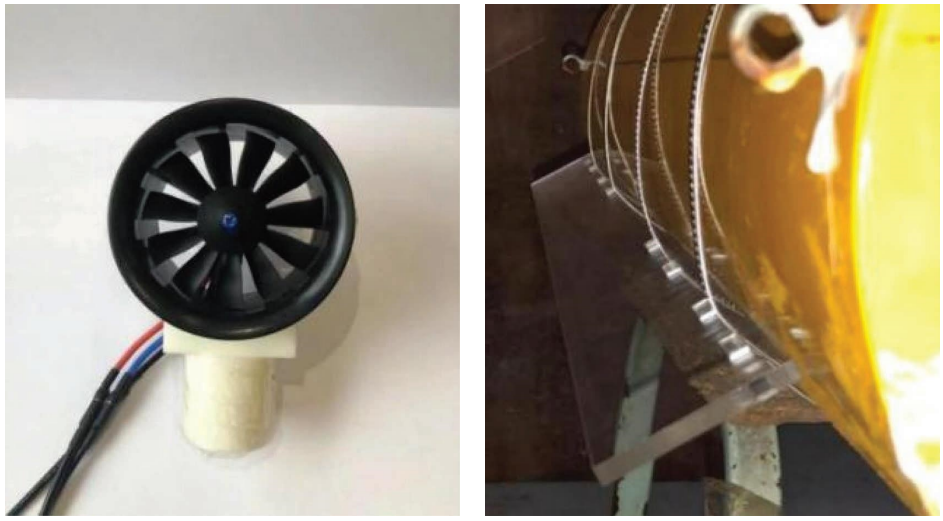

(a) (b)

Figure 4: (a) Culvert wind turbine for the test and (b) installation details of the wing plate.

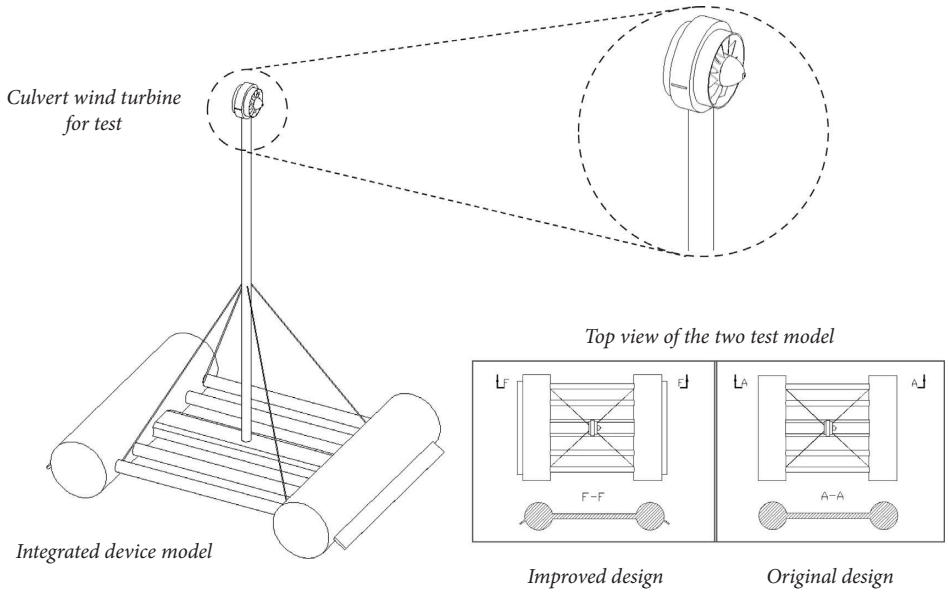

Figure 5: The diagram of the experimental model.

increase in the wave period, the sway motion response amplitudes of both devices increased accordingly. When the wave period is $T > 1.2$ s, the improved device showed a better antisway smoothing effect at different wave heights and its own motion amplitude was small. Compared with the archetype device, the maximum amplitude reduction of the sway amplitude was 19.63%, and the average amplitude reduction was 13.7%. This is because the wing plate increases the resistance of the improved device in the direction of the incoming waves, effectively increasing the restoring force of the device, thus reducing the overall motion of the device and improving the wave suppression performance.

To more intuitively show the influence of the roll motion response amplitude of the integrated device as the wave period changes and to study the effect of the improved device on reducing the roll amplitude, the variation in the roll amplitude with the wave period is shown in Figure 14.

According to the analysis in Figure 14, the variation trend of the roll motion response amplitudes of the improved and archetype devices under the influence of wave period changes is the same. With an increase in the wave period, the roll motion response amplitudes of both devices initially increased and then decreased. For a wave period of $T > 1.2$ s, the roll amplitude increased by an average of 6.3%. By comparison, it was found that there was a corresponding

Figure 6: Overall test model of the integrated device.

Table 5: Test conditions of the integrated device.

Working conditions	Actual working condition		Test working condition	
	Wave period (s)	Wave height (m)	Wave period (s)	Wave height (m)
1	7.75	4.5	1.0	0.075
2	8.5	4.5	1.1	0.075
3	9.3	4.5	1.2	0.075
4	10.075	4.5	1.3	0.075
5	10.85	4.5	1.4	0.075
6	11.625	4.5	1.5	0.075
7	12.4	4.5	1.6	0.075
8	13.175	4.5	1.7	0.075
9	7.75	3	1.0	0.05
10	8.5	3	1.1	0.05
11	9.3	3	1.2	0.05
12	10.075	3	1.3	0.05
13	10.85	3	1.4	0.05
14	11.625	3	1.5	0.05
15	12.4	3	1.6	0.05
16	13.175	3	1.7	0.05

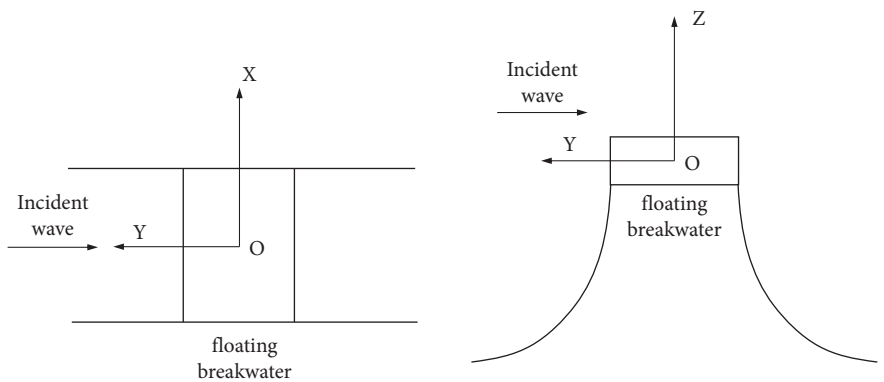

Figure 7: Schematic diagram of the test coordinate system.

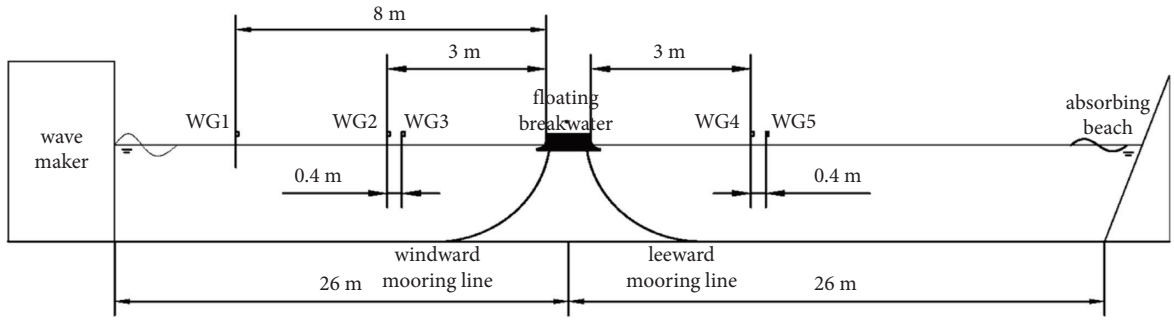

Figure 8: Layout of the wave gauge.

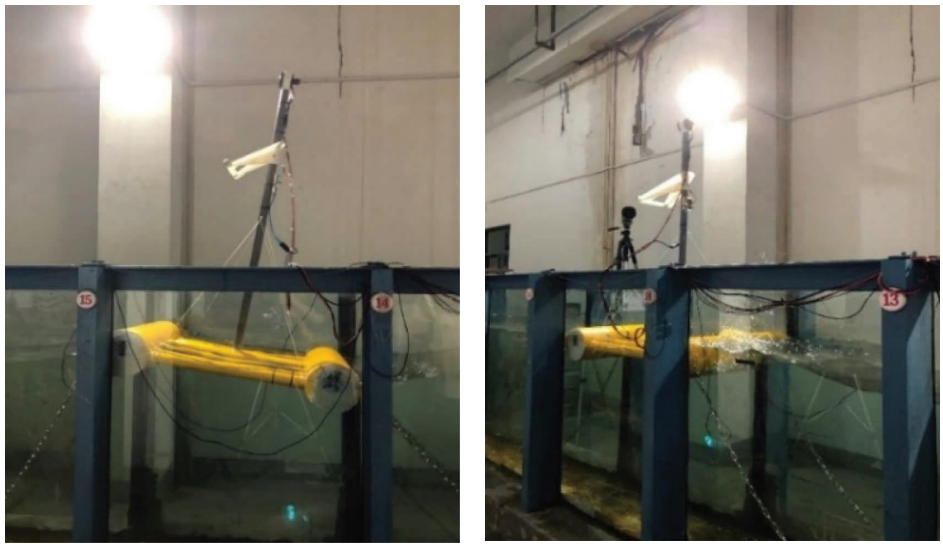

(a) (b)

Figure 9: Photographs in the test. (a) Side view and (b) front view.

relationship between the variation trends of the roll and sway amplitudes of the two devices. When the wave period of the archetype device $T < 1.2$ s, the sway amplitude was less than that of the improved model, whereas the roll amplitude was greater than that of the improved model; the reverse was true when the wave period was greater than 1.2 s. Although the roll amplitude of the improved device is slightly larger than that of the original device under most working conditions, the maximum roll amplitude of the improved device is smaller than that of the original device under different working conditions with the same wave height, indicating that the improved device has certain advantages of being more stable in roll motion.

4.3. Mooring Force Analysis. Aiming at the mooring cable tension of the two types of devices, in this paper, the tension of mooring line acting on the windward and leeward is measured by experiments. The maximum value of mooring force in the stable period was selected for statistics. The mooring force of the integrated device varies with the wave period as shown in Figure 15. The maximum force acting on the windward mooring line was defined as F_W. Similarly, the maximum force acting on the leeward mooring line was defined as F_I.

According to Figure 15, it can be analyzed that under the same working conditions, the mooring force of the improved design is greater than original design. Combined with the abovementioned analysis of motion response results, the improved device shows a better stable effect of reducing sway and heave than the prototype device. Meanwhile, due to its intense roll motion, the improved device needs greater mooring tension to ensure the stability of its own motion. Especially, under the condition of wave period $T > 1.2$ s, the improved device has more severe roll motion than prototype device, which leads to more mooring force of the improved device.

4.4. Analysis of the Wave Elimination Effect. To demonstrate the wave elimination effect of the integrated device more intuitively, the changes in the wave height of the model facing the incident waves and that of the incident waves in the flume were measured experimentally. The two-point method was used to separate the incident and transmission waves and calculate the transmission coefficient.

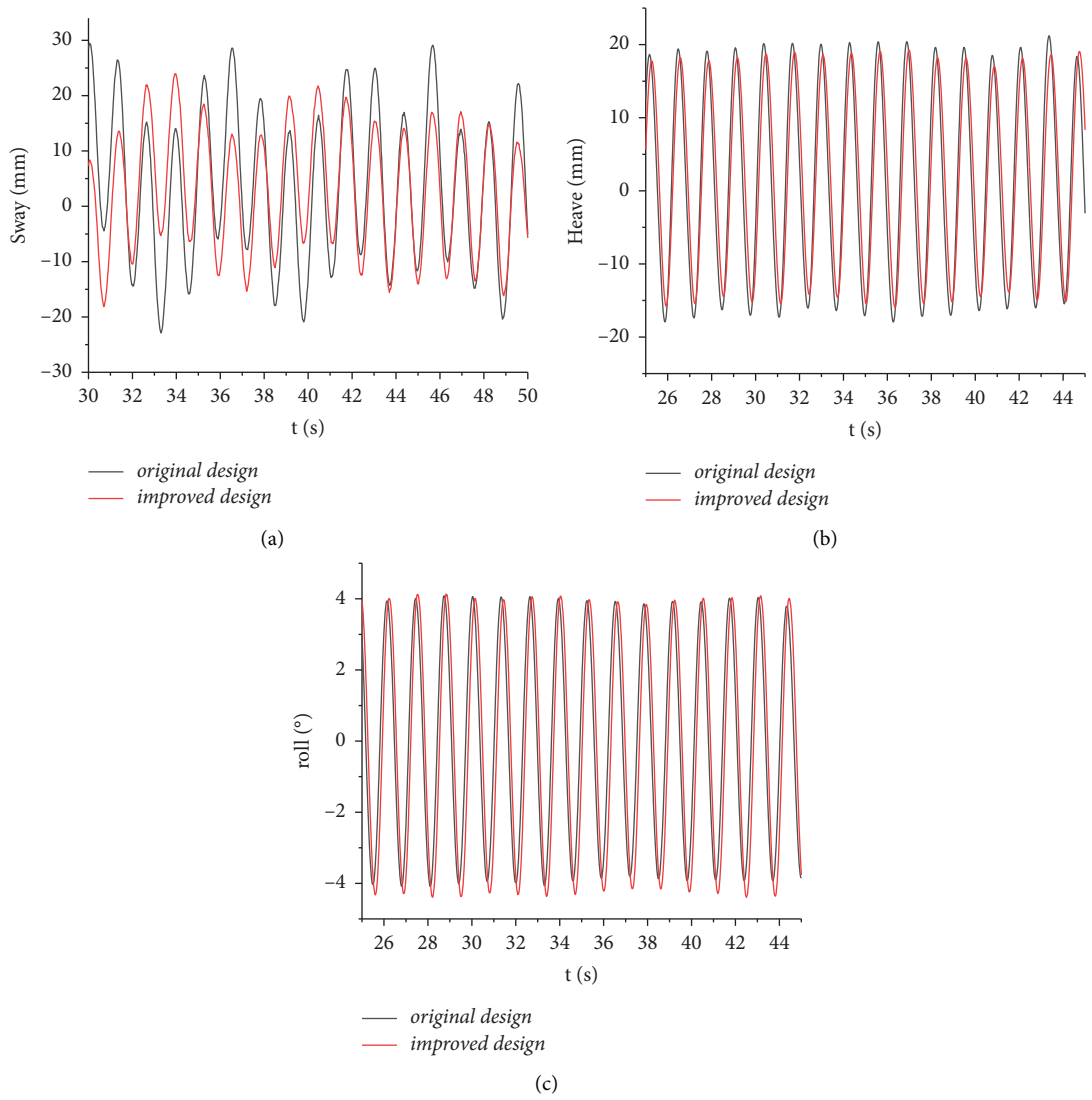

Figure 10: Time history curve of motion response. (a) Sway time history curve, (b) heave time history curve, and (c) roll time history curve.

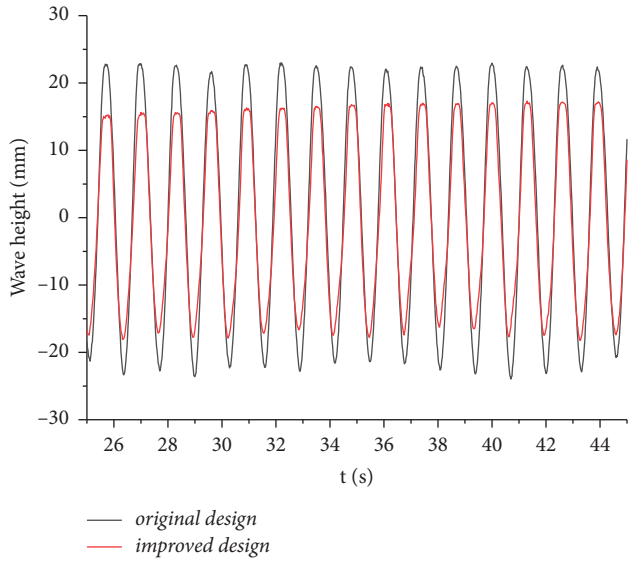

Figure 11: Comparison of the wave height duration curve behind floating breakwater.

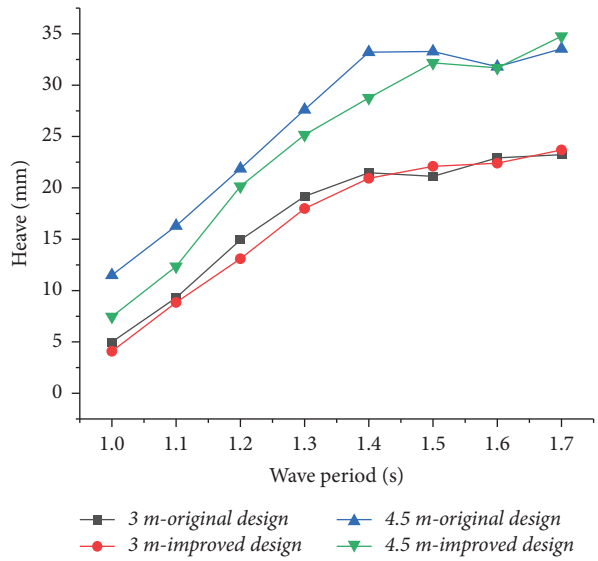

Figure 12: Comparison of heave amplitude variation with the wave period.

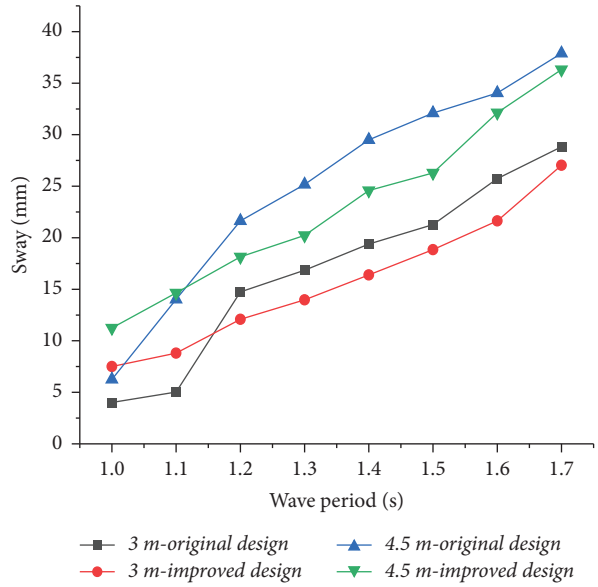

Figure 13: Comparison of sway amplitude variation with the wave period.

The variation in the transmission coefficient with the wave period is shown in Figure 16.

The comparison results in Figure 16 show that under the same working conditions, the transmission coefficient of the improved device was smaller than that of the archetype device and the average amplitude reduction was 28.5%. The wave elimination effect of the improved device was clearly better than that of the archetype device. When the wave period of the archetype device $T < 1.4$ s, the improved model exhibited a more pronounced wave elimination effect, and the transmission coefficient decreased by 51.3% on average compared with that of the archetype. For a wave period $T > 1.4$ s, the improved device also showed an advantage in wave elimination performance, with an average reduction of 5.7%. This is because there are three main wave attenuating mechanisms for floating breakwaters: (1) reflecting the incident waves, (2) breaking waves, and (3) disturbing the motions of the wave particles [33]. The two devices discussed in this paper mainly carry out wave elimination through (1) and (3). Under the same working conditions, the motion amplitude of the improved device is smaller than that of the original device owing to the antisway and stabilizing effect of the wing plate, and the improved device has a more stable wave elimination state, which effectively reflects and dissipates the energy of the incident wave and interferes with its transmission. Combined with the data of mooring force, the large mooring force of the improved device indicates that its own motion is more intense, which enhances its own motion

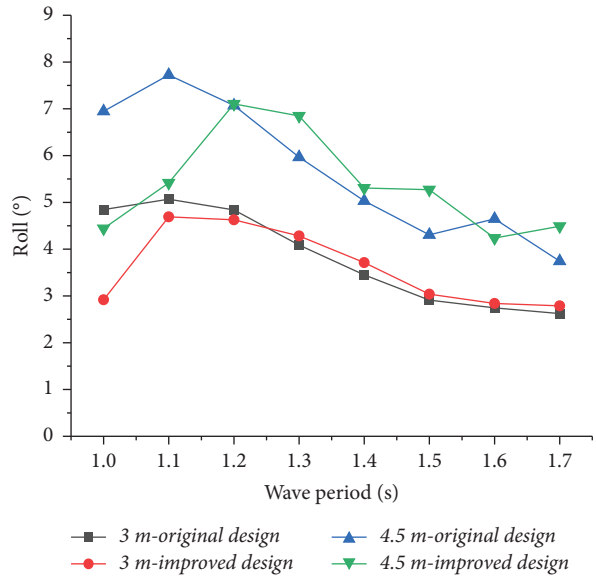

Figure 14: Comparison of roll amplitude variation with the wave period.

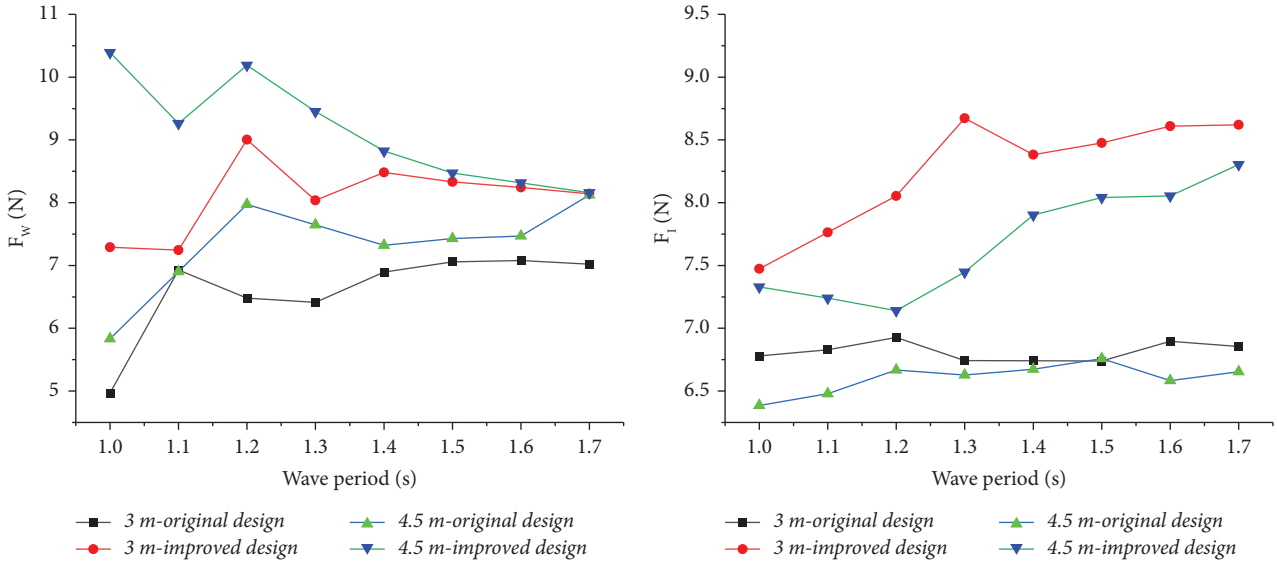

Figure 15: (a) Forces acting on the windward mooring lines of the four test conditions; (b) forces acting on the leeward mooring lines of the four test conditions.

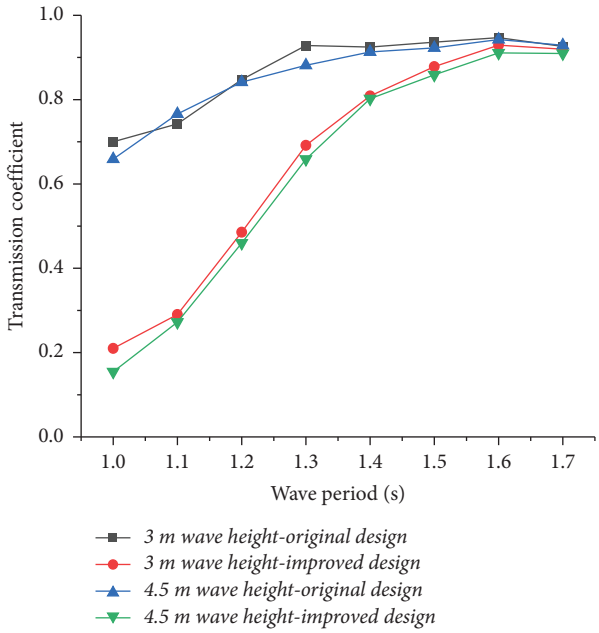

Figure 16: Comparison of transmission coefficient with the wave period.

wave elimination ability, disturbs the movement of water particles to a great extent, and brings better wave elimination performance.

5. Conclusion

This study aims at the design scheme of an integrated device combined with a floating wind turbine based on a floating breakwater, studying its motion response and wave dissipation performance in a two-dimensional test flume and comparing it with the improved device proposed in this paper. The following conclusions were drawn:

(1) The motion response amplitudes of the improved device at different wave heights and periods showed the same variation trend as those of the archetype device. The improved device had a smaller motion amplitude for heave and sway, reflecting better wave-endurance performance and more stable hydrodynamic performance. At the same time, the improved device had a larger roll amplitude and required a larger mooring force to ensure its own stability.

(2) The improved device exhibited a more significant wave-elimination effect. Compared with the archetype device, the transmission coefficient of the improved device has an average reduction of 28.5%, which reflects better wave-attenuation performance. The improved integrated device combines a floating breakwater with a wind power generation device, which not only achieves wave elimination and provides a broad cover water area but can also convert wind energy into electricity and promote the development of offshore wind power, which has significant economic benefits and broad application prospects.

Data Availability

The data used to support the findings of this study are available from the corresponding author upon request.

Conflicts of Interest

The authors declare that there are no conflicts of interest.

Acknowledgments

The authors extend their appreciation to the National Natural Science Foundation of China (grant no. 52071161) for funding this research.

References

[1] gwec, "Global wind report 2022," 2022, https://gwec.net/global-wind-report-2022.

[2] J. O. G. Tande, K. Merz, U. S. Paulsen, and H. G. Svendsen, "Floating offshore turbines," *WIREs Energy and Environment*, vol. 4, no. 3, pp. 213–228, 2015.

[3] S. Roga, S. Bardhan, Y. Kumar, and S. K. Dubey, "Recent technology and challenges of wind energy generation: a review," *Sustainable Energy Technologies and Assessments*, vol. 52, Article ID 102239, 2022.

[4] F. Borisade, T. Choisnet, and P. W. Cheng, "Design study and full scale MBS-CFD simulation of the IDEOL floating offshore wind turbine foundation," *Journal of Physics: Conference Series*, vol. 753, no. 9, Article ID 092002, 2016.

[5] H. Díaz, J. Serna, J. Nieto, and C. Guedes Soares, "Market needs, opportunities and barriers for the floating wind industry," *Journal of Marine Science and Engineering*, vol. 10, no. 7, p. 934, 2022.

[6] M. T. Mikkel, "Force technology," 2014, https://forcetechnology.com/en/cases/windsea-floating-wind-turbine-platforms.

[7] J. M. Jonkman, *Dynamics Modeling and Loads Analysis of an Offshore Floating Wind Turbine*, University of Colorado at Boulder, Boulder, CO, USA, 2007.

[8] J. M. Jonkman and M. L. Buhl, *Fast User's Guide-Updated August 2005. Fast 2005. Tech. Rep*, National Renewable Energy Laboratory (NREL), Golden, Colorado, 2005.

[9] DNVGL, *Digital Solutions Bladed Engineering Feature Summary*, DNVGL: V eritasveien, Norway, Europe, 2020.

[10] Y. Zhou, Q. Xiao, C. Peyrard, and G. Pan, "Assessing focused wave applicability on a coupled aero- hydro-mooring FOWT system using CFD approach," *Ocean Engineering*, vol. 240, Article ID 109987, 2021.

[11] T. T. Tran and D. H. Kim, "The coupled dynamic response computation for a semi-submersible platform of floating offshore wind turbine," *Journal of Wind Engineering and Industrial Aerodynamics*, vol. 147, pp. 104–119, 2015.

[12] H. S. Yang, "Comparison of different fidelity hydrodynamic-aerodynamic coupled simulation code on the 10 MW semi-submersible type floating offshore wind turbine," *Ocean Engineering*, p. 281, 2023.

[13] Y. Shen, X. Zhao, and X. Li, "State of the art in dynamic modeling and load analysis of offshore floating wind turbines," *Hunan Univ Sci Technol (Nat Sci Ed)*, vol. 32, no. 4, pp. 23–31, 2017.

[14] Y. Li, C. Le, H. Ding, P. Zhang, and J. Zhang, "Dynamic response for a submerged floating offshore wind turbine with different mooring configurations," *Journal of Marine Science and Engineering*, vol. 7, no. 4, p. 115, 2019.

[15] H. Wang and Z. Hu, "Research technique and development of coupled dynamic performance of offshore floating wind turbines," *Naval Architecture and Ocean Engineering*, vol. 34, no. 1, pp. 7–14, 2018.
[16] Z. Guo, L. Meng, and Y. Zhao, "Development and method of the offshore floating wind turbines wave-tank model test," *China Offshore Platform*, vol. 31, no. 6, pp. 1–14, 2016.
[17] A. Li, Y. Liu, H. Li, and H. Fang, "Analysis of water wave interaction with a submerged fluid-filled semi-circular membrane breakwater," *Ocean Engineering*, vol. 197, Article ID 106901, 2020.
[18] X. Liu, Y. Liu, P. Lin, and A. Li, "Numerical simulation of wave overtopping above perforated caisson breakwaters," *Coastal Engineering*, vol. 163, Article ID 103795, 2021.
[19] B. Sun, C. Li, S. Yang, H. Zhang, and Z. Song, "Experimental and numerical study on the wave attenuation performance and dynamic response of kelp-box type floating breakwater," *Ocean Engineering*, vol. 263, Article ID 112374, 2022.
[20] B. Nasri, M. N. Moghim, and M. A. Badri, "Experimental study on trapezoidal pontoon-type floating breakwaters with attached porous plates," *J. Ocean Eng. Mar. Energy*, vol. 7, no. 1, pp. 41–57, 2021.
[21] C.-Y. Ji, X. Chen, J. Cui, Z.-M. Yuan, and A. Incecik, "Experimental study of a new type of floating breakwater," *Ocean Engineering*, vol. 105, pp. 295–303, 2015.
[22] C.-Y. Ji, Y. Cheng, K. Yang, and G. Oleg, "Numerical and experimental investigation of hydrodynamic performance of a cylindrical dual pontoon-net floating breakwater," *Coastal Engineering*, vol. 129, pp. 1–16, 2017.
[23] E. D. Christensen, H. B. Bingham, A. P. Skou Friis, A. K. Larsen, and K. L. Jensen, "An experimental and numerical study of floating breakwaters," *Coastal Engineering*, vol. 137, pp. 43–58, 2018.
[24] H. Islam, S. C. Mohapatra, J. Gadelho, and C. Guedes Soares, "OpenFOAM analysis of the wave radiation by a box-type floating structure," *Ocean Engineering*, vol. 193, Article ID 106532, 2019.
[25] J. Cui, X. Chen, P. Sun, and M. Li, "Numerical investigation on the hydrodynamic behavior of a floating breakwater with moon pool through a coupling SPH model," *Ocean Engineering*, vol. 248, Article ID 110849, 2022.
[26] X. L. Zhao, D. Z. Ning, Q. P. Zou, D. S. Qiao, and S. Q. Cai, "Hybrid floating breakwater-WEC system: a review," *Ocean Engineering*, vol. 186, Article ID 106126, 2019.
[27] P. A. Galvani, F. Sun, and K. Turkoglu, "Aerodynamic modelling of the nrel 5-mw wind turbine for nonlinear control system design: a case study based on real-time nonlinear receding horizon control," *Aerospace*, vol. 3, 2016.
[28] Y. K. Chen, Y. Liu, D. D. Meringolo, and J. M. Hu, "Study on the hydrodynamics of a twin floating breakwater by using SPH method," *Coastal Engineering*, vol. 179, Article ID 104230, 2023.
[29] L. Li, Y. Gao, Z. Hu, Z. Yuan, S. Day, and H. Li, "Model test research of a semisubmersible floating wind turbine with an improved deficient thrust force correction approach," *Renewable Energy*, vol. 119, pp. 95–105, 2018.
[30] L. Wan, M. Greco, C. Lugni, Z. Gao, and T. Moan, "A combined wind and wave energy-converter concept in survival mode: numerical and experimental study in regular waves with a focus on water entry and exit," *Applied Ocean Research*, vol. 63, pp. 200–216, 2017.
[31] E. Oguz, D. Clelland, A. H. Day et al., "Experimental and numerical analysis of a tlp floating offshore wind turbine," *Ocean Engineering*, vol. 147, pp. 591–605, 2018.
[32] H. K. Chang and T. W. Hsu, "A two-point method for estimating wave reflection over a sloping beach," *Ocean Engineering*, vol. 30, no. 14, pp. 1833–1847, 2003.
[33] C. Ji, X. Deng, and Y. Cheng, "An experimental study of double-row floating breakwaters," *Journal of Marine Science and Technology*, vol. 24, no. 2, pp. 359–371, 2019.